Journal of Tropical Forest Science 36(4): 379–390 (2024)
https://doi.org/10.26525/jtfs2024.36.4.379
ISSN: 0128-1283, eISSN: 2521-9847

SYNTHESIS, CHARACTERISATION AND APPLICATION OF ACTIVATED CARBON AS A SMOKE FILTER

Norli U[1], Nor Kartini AB[2,*] & Cheng SF[1]

[1] *Unit of Research on Lipids (URL), Chemistry Department, Faculty of Science, Universiti Malaya, 50603 Kuala Lumpur, Malaysia*
[2] *Chemistry Department, Faculty of Science, Universiti Malaya, 50603 Kuala Lumpur, Malaysia*

**kartini@um.edu.my*

Submitted December 2023; accepted July 2024

Activated carbon (AC) synthesis and application have been extensively studied. However, reports on its deployment in smoke particle filters are limited. The present study synthesised AC from two agricultural wastes, namely coconut shell (CS) and palm kernel shell (PKS). The AC was incorporated into a custom-made smoke muffler to filter smoke from paddy straw combustion. Phosphoric acid, potassium hydroxide and zinc chloride were employed to produce the AC via a physicochemical method. CS and PKS were subjected to microwave radiation, a one-to-one (1:1) activation ratio, 30 min of impregnation time, and 4 min of radiation. Background studies were conducted on the starting materials, including lignocellulosic content and proximal and ultimate evaluations. The AC samples procured were characterised with Fourier Transform infrared (FTIR), Brunauer, Emmett, and Teller (BET) surface area, and field emission scanning electron microscope (FESEM) analyses. The zinc chloride-activated CS (MZCS) produced the optimal AC under minimal conditions, documenting a 391.26 m^2 g^{-1} BET surface area. Based on FESEM results, the MZCS distributed smoke particles evenly, demonstrating smoke adsorbent abilities. The results also indicated a favourable physical interaction between the surface and smoke particles. Conclusively, the MZCS possesses potential as a smoke filter.

Keywords: Activated carbon, agricultural waste, coconut shell, palm kernel shell, smoke filter

INTRODUCTION

Agriculture is a global and rapidly increasing industry with a total of 22% of agricultural wastes generated during production, processing, and storage (Atinkut et al. 2020). According to Akbari et al. (2021), open-burning crop waste is the simplest and economically feasible method for disposing of agricultural refuse. Post-crop harvest field waste burning is widely practised in several Southeast Asian countries. The activity releases significant volumes of harmful air pollutants (Tipayarom & Kim Oanh 2020). For instance, the smoke from biomass burning in Kalimantan, Indonesia, accounted for 59% of PM2.5 (Stampfer et al. 2020).

The soot particles released with the smoke from burning vary from 10 µm to under 1 µm (Phairuang et al. 2019, Pósfai et al. 2003). A smoke trapping system utilising activated carbon (AC) could be introduced to filter smoke emission through an adsorption mechanism to mitigate the detrimental effects of burning. Nevertheless, most reports on AC applications have focused on aqueous adsorption, such as dye, methyl blue, wastewater treatment, and dye removal (Yaacoubi & Songlin 2019).

The current study assessed a novel and unique utilisation of activated carbon (AC), its capability to adsorb soot. The present study aimed to synthesise AC from coconut shells (CS) and palm kernel shells (PKS). The applicability of the AC samples as smoke particle filters was evaluated for paddy straw combustion. A custom-made smoke muffler and paddy husks as the smoke source were also utilised. Three commonly employed activating agents, phosphoric acid (H_3PO_4), potassium hydroxide (KOH), and zinc chloride ($ZnCl_2$), were utilised to prepare the AC samples. The activation agents were impregnated into the biomass materials before subjecting the specimens to microwave radiation. The surface morphology of the samples after combustion were also evaluated.

MATERIALS AND METHODS

Materials

The palm kernel shells (PKS) employed in the present study were collected from Sime Darby Plantation, Pulau Carey, Selangor. At the same time, coconut shells (CS) were procured from the coconut milk industry in Kampung Telaga Air, Kuching Sarawak, Malaysia. A paddy field in Kangar, Perlis, Malaysia, supplied the paddy straws. Analytical grade chemicals and reagents were also utilised.

Methodology

A PE 2400 Series II CHNS/O Elemental Analyzer was employed for carbon, hydrogen, nitrogen, sulfur/oxygen (CHNS/O) analysis, while Fourier transform infrared (FTIR) assessment was performed with a Perkin Elmer FTIR Spectrum 400 with attenuated total reflection (ATR) extension. The Brunauer, Emmett, and Teller (BET) surface areas of the AC samples produced in this study were analysed using the Advance Surface Area and Porosity Analyzer Micromeritics TriStar II Plus with nitrogen (N_2) gas as the carrier gas. An SU8220 (Hitachi Brand) field emission scanning electron microscope (FESEM) was employed to evaluate the surface morphology of the specimens. The microwave used for preparing the AC samples was a Panasonic NN-CD997S with a 42 L capacity.

The present study conducted a proximal analysis to determine the moisture and ash contents of the AC specimens based on methods D4442 and E1775, respectively, outlined by the American Society for Testing and Materials (ASTM). For moisture content evaluation, approximately 2 g (m_1) of starting materials was weighed and oven-dried at 102 °C until a constant mass was obtained and recorded (m_2). Finally, moisture content was calculated according to Equation (1). Ash content analysis was initiated by heating the dried AC samples (m_3) in an electrical furnace at 650 °C for 3 h. The residual ash was cooled in a desiccator before recording the final weight (m_4). Equation (2) was employed to determine the ash contents of the specimens.

$$\text{Moisture (\%)} \frac{m_1 - m_2}{m_1} \times 100 \quad (1)$$

$$\text{Ash (\%)} = \frac{m_4}{m_3} \times 100 \quad (2)$$

The biomass (PKS and CS) employed in this study was leached with a 2:1 v/v benzene and ethanol mixture at room temperature for 3 h. Subsequently, the substances were oven dried at 110 °C until a constant mass was recorded. The initial (m_5) and dry (m_6) masses of the sample were also documented before determining the mass difference. In this study, the mass difference denoted the extractive amount, calculated per Equation (3).

$$\text{Extractive amount} = \frac{m_5 - m_6}{m_5} \times 100\% \quad (3)$$

The lignocellulosic contents of the starting material in this study were calculated based on their extractive, hemicellulose, lignin, and cellulose levels. The procedure adopted in the present study was according to the methodology outlined by Li et al. (2004). Approximately 1 g of extractive-free biomass (m_7) was placed in a conical flask before adding 150 mL of NaOH solution (20 g L^{-1}). The mixture was boiled for 3.5 h and filtered. Subsequently, the biomass was washed with distilled water until the pH of the filtrate reached seven and oven-dried at 110 °C until a constant mass was recorded (m_8). The difference in mass is the hemicellulose content of the biomass specimens, calculated per Equation (4).

$$\text{Hemicellulose content} = \frac{m_7 - m_8}{m_7} \times 100\% \quad (4)$$

Approximately 5 g (m_9) of the biomass was soaked in 72% sulphuric acid at room temperature for 2 h. Subsequently, the substance was refluxed at 100 °C for 2 h, filtered, washed with distilled water, and oven-dried at 105 °C. The dry mass (m_{10}) of the shells was recorded and utilised to determine their lignin content as in Equation (5). The difference in extractives, hemicellulose, lignin, and cellulose

levels was employed to determine the cellulose content of the biomass using Equation (6). The current study assumed that only the extractives, hemicellulose, lignin, and cellulose exist in the biomass for the calculation.

$$\text{Lignin content} = \frac{m_9 - m_{10}}{m_9} \times 100\% \quad (5)$$

$$\text{Cellulose content} = 100 - (\text{Extractives} + \text{hemicellulose} + \text{lignin}) \text{ contents} \quad (6)$$

The parameters adopted in the present study were based on the report by Kumar et al. (2020) and applied without a prior optimisation study. Firstly, the agricultural wastes, PKS and CS, were cleaned and dried. A Carbolite Gero HTF 17/5 furnace was employed to heat the shells for 30 min at temperatures between 600 °C and 650 °C. The charred products were subjected to microwave radiation for 4 min at 700 W post separate activations with H_3PO_4, KOH, and $ZnCl_2$.

The AC samples procured were washed with distilled water and dried. The AC percentage yield was determined to indicate process efficiency according to Equation (7). Henceforth, the acid-, base-, and $ZnCl_2$-activated microwave radiated samples were denoted MA, MB, and MZ, respectively. Accordingly, MAPKS represented the acid and microwave-activated PKS AC sample.

$$\text{Yield} = \frac{\text{Mass after activation (g)}}{\text{Original mass (g)}} \times 100\% \quad (7)$$

The current study utilised a custom-made smoke filter to evaluate the synthesised AC performance. A 0.1 g AC was loaded on the holder in the smoke filter before combusting the rice straws in a burning chamber (Figure 4). The paddy straws were burned continuously for two scales of combustion: 30 min for 50 g of straw and 60 min for 100 g of straw.

RESULTS AND DISCUSSION

Proximate analysis is performed to determine the energy conversion capabilities of biomass (Sanchez-Silva et al. 2012). In this study, moisture, ash, volatile matter, and fixed carbon contents of the biomass samples were assessed. Moisture refers to the amount of water in biomass. Pisupati and Krishnamoorthy (2017) proposed that biomass should contain under 2% moisture to ensure fine char particle developments. The moisture contents of the PKS and CS samples were 6.47 and 5.64%, respectively (Table 1). The raw materials employed in the present study were heated until a constant mass was recorded before initiating the carbonisation process to produce a better char.

Table 1 The proximate and ultimate analysis results of the starting materials

Content (% w/w)	PKS	CS
Moisture	6.47	5.64
Ash	2.16	0.24
Volatile matter	72.13	79.63
Fixed carbon	19.24	14.49
Carbon	43.37	47.07
Hydrogen	16.69	13.16
Nitrogen	0.90	0.36
Sulphur	1.69	1.68
Oxygen	41.25	37.73

PKS = palm kernel shell, CS = coconut shell

Ash value indicates the amount of inorganic residue remaining in biomass post-combustion. Primarily, ash comprises silica, aluminium, iron, calcium, and traces of magnesium, sodium, and potassium (Basu 2018). Ash is heat-resistant, which could prevent organic molecule decomposition (Enders et al. 2012). Consequently, increased carbonisation temperature might be due to a high ash concentration. The PKS documented a higher ash concentration (2.16%) than CS (0.24%), thus requiring a greater carbonisation temperature. The observations also indicated that a considerable ash content leads to a high heating value.

Volatile matter is the gas weight percentage emitted by a substance after being heated at high temperatures. Accordingly, substances with high volatile matter values would produce reduced percentage yield due to the significant amounts of gas produced during carbonisation. The results in the present study supported the hypothesis (Table 1). The PKS, which had a lower volatile matter (72.13%), yielded more product than the CS specimen.

Fixed carbon knowledge aids combustion equipment selections in large-scale AC productions, considering starting material hardness provides information about biomass caking properties (Sarkar 2015). Fixed carbon content is the residue that remains after the volatile contents in a substance have been released following high-temperature combustions. A more significant fixed carbon content would produce higher char formation and yield. Although fixed carbon primarily comprises carbon, it also consists of trace amounts of hydrogen, oxygen, nitrogen, and sulphur, which are not released with the emitted gases.

Biomass chemical energy could be calculated by determining its fixed carbon to volatile matter proportions. The information also reflects the convertibility of the biomass into energy (Sanchez-Silva et al. 2012). Although significant levels of volatile matter over fixed carbon indicate that the biomass could release high energy, significant operational costs to burn and process biomass are required (Sanchez-Silva et al. 2012). In the current study, the proportion of fixed carbon is lower in the CS (14.49%) than in the PKS sample (19.24%). The volatile matter in the CS is high, at 79.63%. The volatile matter of CS in this study is consistent as recorded by Mohd Iqbaldin et al. (2013). A higher volatile matter with low fixed carbon results in CS having a lower operational cost and consume less energy than PKS.

In this study, the CHNS/O contents of the starting materials were analysed to assess their carbon, hydrogen, nitrogen, sulphur, and oxygen levels. Table 1 summarises the CHNS/O contents of PKS and CS. The hydrogen-to-carbon (H/C) ratios of the PKS and CS samples were 0.29 and 0.28, respectively, while the oxygen-to-carbon (O/C) ratios were 0.95 and 0.80. Low H/C and O/C values are preferred to obtain lower heating values (Soh et al. 2019). Based on the results, the CS specimen would record a lower heating value than PKS.

The lignocellulosic contents of the starting materials employed in the present study were determined to understand the characteristics of the biomass further. Table 2 lists the lignocellulosic contents of the PKS and CS employed in this study. Lignin was the predominant biopolymer in PKS, whereas the CS sample was primarily hemicellulose. The CS specimen also contained more hemicellulose than PKS, 38.89% and 29.80%, respectively. On the other hand, the PKS recorded a higher lignin content, 40.67%, than CS, 33.07%. The results were similar to the findings reported by Ruqayah et al. (2014).

Table 2 The lignocellulosic contents of the PKS and CS samples

Content (%)	PKS	CS
Hemicellulose	29.80	38.89
Lignin	40.67	33.07
Cellulose	13.68	16.00
Extractives	5.53	5.14

PKS = palm kernel shell, CS = coconut shell

Lignin is a rigid structure that binds polysaccharide fibres and is a more heat-resistant component than hemicellulose and cellulose (Dhyani & Bhaskar 2018). The PKS sample evaluated in the current study recorded a higher lignin level than CS, 40.67 and 33.07%, respectively. Consequently, a higher temperature was required to carbonise PKS (Ahmed & Hameed 2020, Wang et al. 2019). The more significant lignocellulosic, O/C, H/C, and ash levels in the PKS contributed to its considerable carbonisation temperature.

Wang et al. (2019) suggested that carbonised biomass should exhibit significant signal loss due to functional group fragmenting and degrading to form carbon skeletons. The present study compared the FTIR spectra of the raw and carbonised biomass samples (Figure 1). The raw FTIR spectra demonstrated no changes when the carbonisation temperature employed was lower than the optimised temperature. The ideal carbonisation temperatures of the PKS and CS specimens were 650 °C and 600 °C, respectively.

The carbonisation duration for each biomass sample was evaluated up to the loss of the FTIR signal. No additional signal loss was observed when the period was increased from 30 to 60 min. Consequently, the present study maintained carbonisation temperature at 30 min, in line with the green technology approach. Commonly, a higher carbonisation temperature is compensated with a shorter duration. For

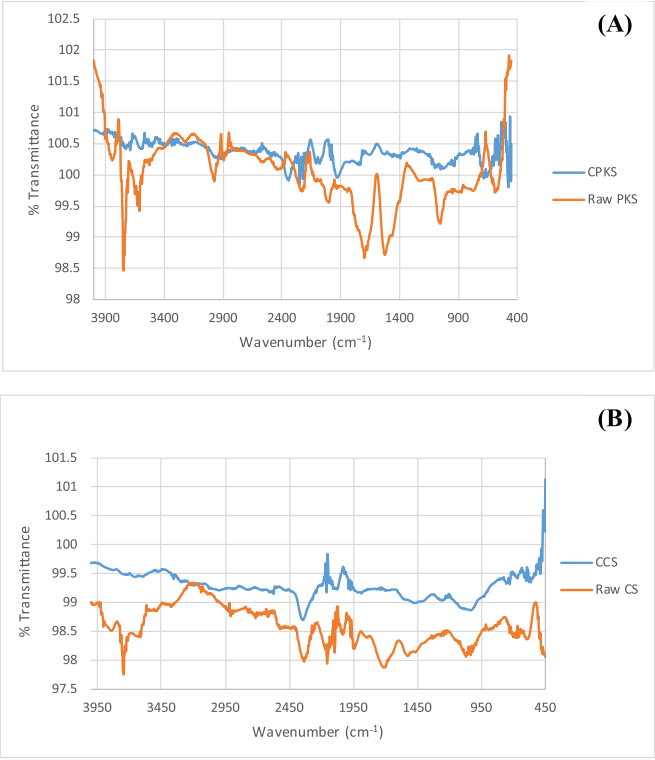

Figure 1 The FTIR spectra of the (A) raw PKS and carbonised PKS (CPKS) and (B) raw CS and carbonised CS (CCS)

instance, Nasri et al. (2019) carbonised CS at 700 °C for 45 min, while Liew et al. (2019) PKS produced AC at 607 °C within 35 min. Nonetheless, the activation time reported in Nasri et al. (2019) and Liew et al. (2019)PKS was 24 h compared to 2 h in this study.

The percentage yields of the CS and PKS samples post-activation are tabulated in Table 3. Carbonisation of the CS specimen occurred until at 600 °C, where the process halted as the carbon skeletal was successfully formed. The reduced FTIR signal proved the hypothesis. For PKS, 650 °C was the optimal carbonisation temperature. No further carbonisation percentage yield evaluation was conducted beyond the ideal temperature.

Carbonisation temperature is critical to ensure successful AC production. Optimal temperature promotes pore structure development (Sanni et al. 2017). Carbonisation at low temperatures (below 300 °C) is too low for biomass volatilisation (Ello et al. 2013). Furthermore, pore structures would not form despite the large yield due to incomplete reaction. Conversely, output is decreased if the temperature is too high (Ello et al. 2013, Yang et al. 2010). The phenomenon results from accelerated reaction rates, leading to lignocellulosic polymer decomposition and fragment burning (Jadhav & Mohanraj 2016). High temperatures also break C–O–C and C–C chemical bonds, decreasing yield (Foo & Hameed 2012).

The PKS utilised in this study recorded a higher percentage yield than CS. The rigidity and resistance to reactions of the PKS were due to its primary component, lignin. The significant H/C and O/C ratio fixed carbon proportion contributes to the endurance of the biomass. An AC percentage yield of 22–25% recorded in the current study was comparable to the reports by Yang et al. (2010), Ghazali &Abdullah (2012), Zailani et al. (2013), and Hidayu & Muda (2016).

The zinc chloride-activated CS (MZCS) procured in the present study registered the highest surface area (391.26 m^2 g^{-1}) and pore volume (0.17 m^3 g^{-1}). Nonetheless, the pore diameter of the sample, 1.69 nm, was significantly smaller than its counterpart, the zinc chloride-activated PKS (MZPKS), at 1.72 nm. The MZPKS also documented a high surface

Table 3 The BET values and percentage yields of the synthesised activated carbon

Parameter	MACS	MBCS	MZCS	MAPKS	MBPKS	MZPKS
BET surface area (m^2/g)	3.93	77.45	391.26	2.88	348.19	367.12
Pore diameter (nm)	1.50	2.20	1.69	0.38	0.38	1.72
Pore volume (m^3/g)	0.001	0.04	0.17	0.0002	0.12	0.16
Percentage yield (%)	17.6	20.5	21.4	17.6	27.3	25

MACS = microwave acid activated coconut shell, MBCS = microwave base activated coconut shell, MZCS = microwave zinc activated coconut shell, MAPKS = microwave acid activated palm kernel shell, MBPKS = microwave base activated palm kernel shell, MZPKS = microwave zinc activated palm kernel shell; BET = Brunauer, Emmett and Teller

area of 339.42 m^2 g^{-1}. The results indicated that activation with $ZnCl_2$ produced AC with a superior surface area than the other activators utilised in this study. Dehydration, electrolytic breakdown, and polymer decomposition were also induced by $ZnCl_2$ (Ma 2017, Saka 2012, Prauchner et al. 2016).

The KOH activation in the present study produced a range of results for both starting materials. The PKS had a high surface area, 328.6 m^2 g^{-1}, while the CS samples documented 77.45 m^2 g^{-1}. The phenomenon was attributable to the rigid lignin content of the MBPKS. The CS was more vulnerable to KOH attacks as it was high in hemicellulose and cellulose. Nevertheless, the pore diameter of both biomass was identical, 2.2 nm, which could result in similar surface reactions. The FESEM images also revealed that the MBPKS and MBCS exhibited hollow cores in Figures 2(B) and 3(B). The pores might have perforated through the biomass due to the rapid reaction during pore formation. As a result, the surface area was reduced while the pore diameter remained constant.

In the present study, acid activation produced AC with the lowest BET. Figures 2(C) and 3(C) illustrate the FESEM images of the H_3PO_4-activated AC samples. The pores on the samples formed tunnels that penetrated through the entire biomass from their upper surfaces. The acid caused an immediate reaction upon contact with the biomass by attacking hemicellulose, which is prone to acid attacks (Jadhav & Mohanraj 2016). Furthermore, H_3PO_4 split the cellulose fibres and depolymerised the hemicellulose and lignin in the specimens (Sanni et al. 2017).

Numerous pores were observed on the surfaces of the acid-activated AC obtained in this study (Figures 2(C) and 3(C)). Nonetheless, due to the aggressive nature of acid activation, the reaction continued until the AC structure was broken. The surface areas of the H_3PO_4-activated AC were low due to perforation. Ilomuanya et al. (2016) and Tounsadi et al. (2016) revealed that acid activation would lead to mesopore formation. Furthermore, performing physical activation post-acid activation would result in the conversion of micropores to mesopores (Tounsadi et al. 2016). Radiation treatment would also lead to rapid expansion of pores, resulting in wall disruptions (Shukla et al. 2020).

The findings in the present study indicated that pore formation on AC depends on the activation type. The optimal pore size was recorded on the $ZnCl_2$-activated AC. The $ZnCl_2$ broke down biomolecules and promoted pore formation (Prauchner et al. 2016, Saka 2012), favouring the desired AC. The chemical also produced AC specimens with the highest BET surface area and uniform pores. A superior surface area was observed on the PKS specimen, documenting 348.19 m^2 g^{-1}, almost identical to the AC with the highest surface area, MZPKS. Nevertheless, activation with KOH did not form high surface-area AC when CS was employed as the starting material. Activation with H_3PO_4 resulted in the least surface area values for both biomasses.

The FESEM images of the carbonised and activated biomass in this study were procured to examine the physical surface structures of each sample. Carbon skeletal formation was visible in the CPKS and CCS specimens (Figures 2(A) and 3(A)). Pores and the simplest form of carbon bodies are formed following biopolymer fragmentation and degradation (Prauchner et al. 2016). Optimal temperatures allow the synthesis of carbon skeletons. On the other

hand, additional pores formed on AC surfaces during activation, contributing to adsorption attributes.

Figures 2(B) and 3(B) demonstrate the base and microwave-activated AC samples. A comparison of the carbonised morphology of the specimens in this study revealed that pores were formed on the biomass surfaces following successful activations. The MBPKS (Figure 2(B)) exhibited more pores on its surfaces, whereas the MBCS (Figure 3(C)) had hollow and damaged pore walls. The finding explained why the MBCS recorded a lower BET than MBPKS. The results also indicated that excessive reaction could destroy pores, forming tunnelled and hollowed AC.

The FESEM images of the MACS and MAPKS AC (Figures 2(C) and 3(C)) demonstrate cell wall disruption and pore narrowing, which penetrated the entire biomass. Biomass structure hollowing was also observed in the acid-activated samples. The phenomenon reduced the surface area of the specimens, where the MACS documented a remarkably low BET of 3.93 $m^2 g^{-1}$.

Figures 2(D) and 3(D) illustrate the pores formed throughout the surfaces of the metal salt AC. The MZCS surface morphology revealed densely packed pores on its surfaces. The specimen also had the highest BET value, 391.26 $m^2 g^{-1}$. Furthermore, no hollowing, aggression, or disruption of pore walls were observed in the MZCS. The findings indicated that the reaction between biomass and $ZnCl_2$ was more favourable than the other activators.

The morphology of the AC surfaces indicated that pore formation was distinct post-activation, regardless of the activating agent utilised. In this study, the $ZnCl_2$-activated AC had pores (Figures 2(D) and 3(D)). The same activator also produced the AC with the highest BET. Nonetheless, when comparing between starting materials, the MZCS demonstrated uniform pores throughout its surfaces (Figure 3(D)).

Applying the synthesised activated carbon as smoke filters

The activated carbon (AC) manufactured in the present study were evaluated in a custom-made steel smoke muffler (Figure 4). The smoke muffler was 40 cm tall and 25.4 cm wide. The equipment could hold up to 500 g of rice paddy straw. The narrow top of the muffler was designed to allow smoke to pass through the AC samples installed in the AC holder, which had up to 5 g capacity.

Soot obtained from FESEM shows that it consists 20% more oxygen (Table 4). In this

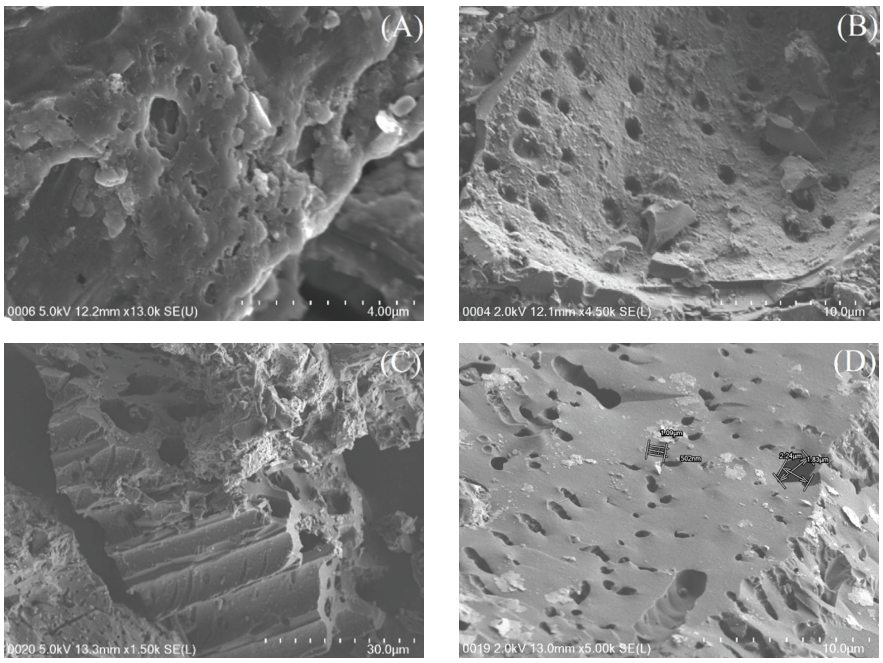

Figure 2 FESEM images of PKS AC; (A) PKS carbonised at 650 ˚C for 30 min followed by 2 h of chemical activation with (B) KOH, (C) H_3PO_4, and (D) $ZnCl_2$ and microwave radiation for 4 min

study, the EDX data of the soot sediments (Table 4) were employed as a reference to identify the soot adsorbed on the surface of the MZCS. The current study aimed to prepare AC that is applicable as a smoke filter capable of particle adsorption, particularly soot from paddy straw combustion. Ideally, the micro- and macropores on an AC should be between 10 µm and under 1 µm to capture soot particles.

The MZPKS and MZCS AC were selected for smoke adsorption evaluations, as the samples documented a surface area of 367.12 and 391.26 $m^2 g^{-1}$, respectively (Table 3). Based on the FESEM measurements, the MZPKS AC had pores between 2.24 µm and 502 nm (Figure 2(D)), while the MZCS recorded pores of 12.2 µm and 948 nm (Figure 3(D)). The MZCS and MZPKS produced in the present study were suitable for smoke particle adsorption, considering that their surface areas and pore sizes were within the range of the particle size intended for capture.

Figure 5(B) illustrates the surface morphology of the AC after being subjected to 30 min of the smoke from paddy straw combustion. The smoke particles were observed to have adhered to the surfaces of the sample surfaces completely. Smoke particles settled evenly across the MZCS surfaces and inside the pores, indicating that the surfaces and smoke particles interacted well. Physically, the MZCS demonstrated a higher adsorption capacity for smoke particles than the MZPKS. Conversely, smoke particles were not evenly adsorbed onto the surfaces of the MZPKS (Figure 5(E)). The observations revealed that the MZCS was suitable as a smoke filter.

Smoke particles clumped and concentrated on the surfaces of the AC until they were not visible (Figure 5(C)) when the combustion was performed for 60 min using 100 g of paddy straw. The findings indicated that increasing the combustion period and paddy straw amount reduced the adsorption capacity of the specimens. Rising combustion time would result in more smoke particles adhering to the AC surfaces and eventually completely covering them. The surfaces would then be unable to trap any more smoke particles. To ensure the surface of AC is not entirely occupied by smoke, employing the amount of AC per gram of combustion material would ensure adsorption efficiency.

Adsorbate accumulation on the AC surfaces indicated physical adsorption. The physisorption of soot particles was homogenous, considering that the adsorbed particles were observable via FESEM. Furthermore, the instantaneous adsorption following combustion suggested physical adsorption.

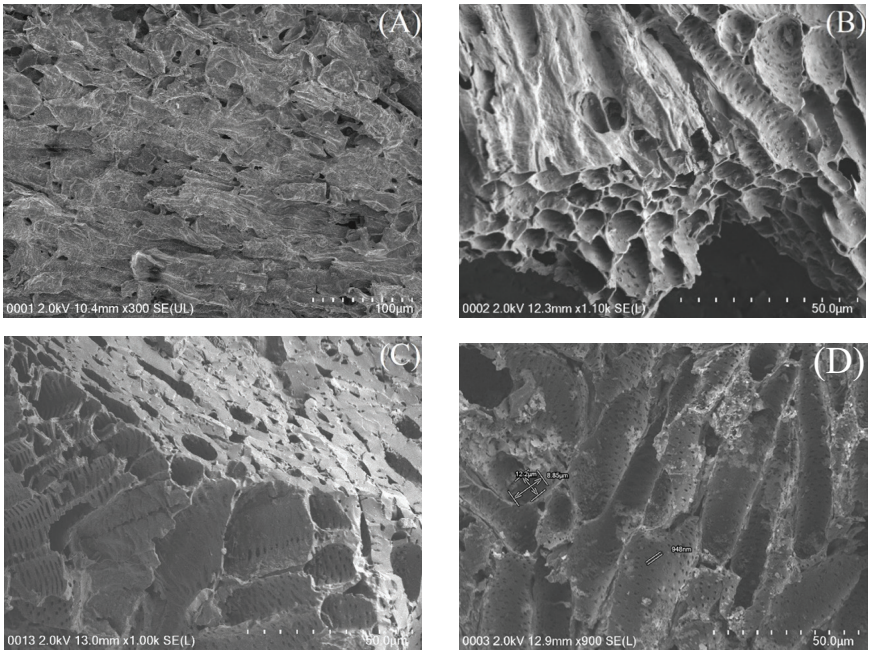

Figure 3 FESEM images of CS AC; (A) CS carbonised at 600˚C for 30 min followed by chemical activation for 2 h with (B) KOH, (C) H_3PO_4, and (D) $ZnCl_2$ and 4 min of microwave radiation

Table 4 The carbon and oxygen content of soot resulted from burning of paddy straw

Sample	Carbon content (%)	Oxygen content (%)
Soot	74.30	22.64
MZCS surface	89.83	9.67
MZCS on soot area	72.49	24.66

MZCS = microwave zinc activated coconut shell

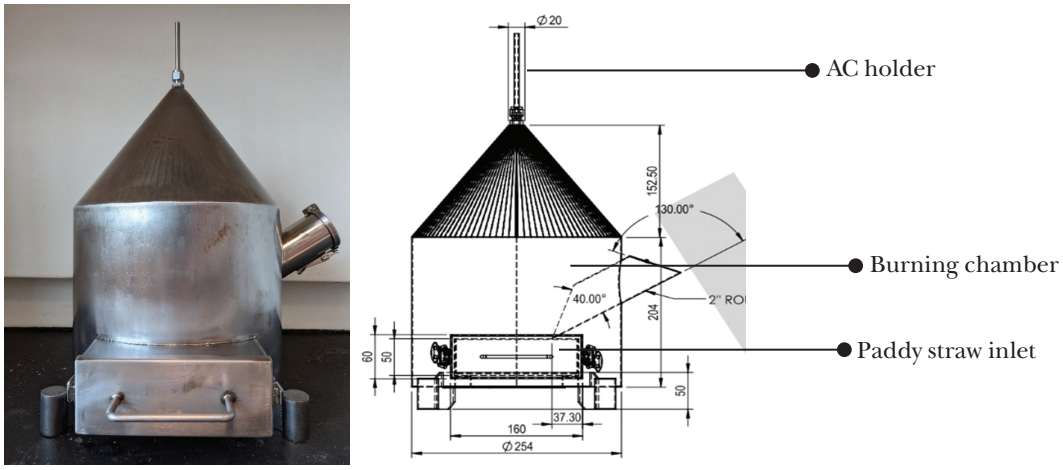

Figure 4 The muffler burning chamber

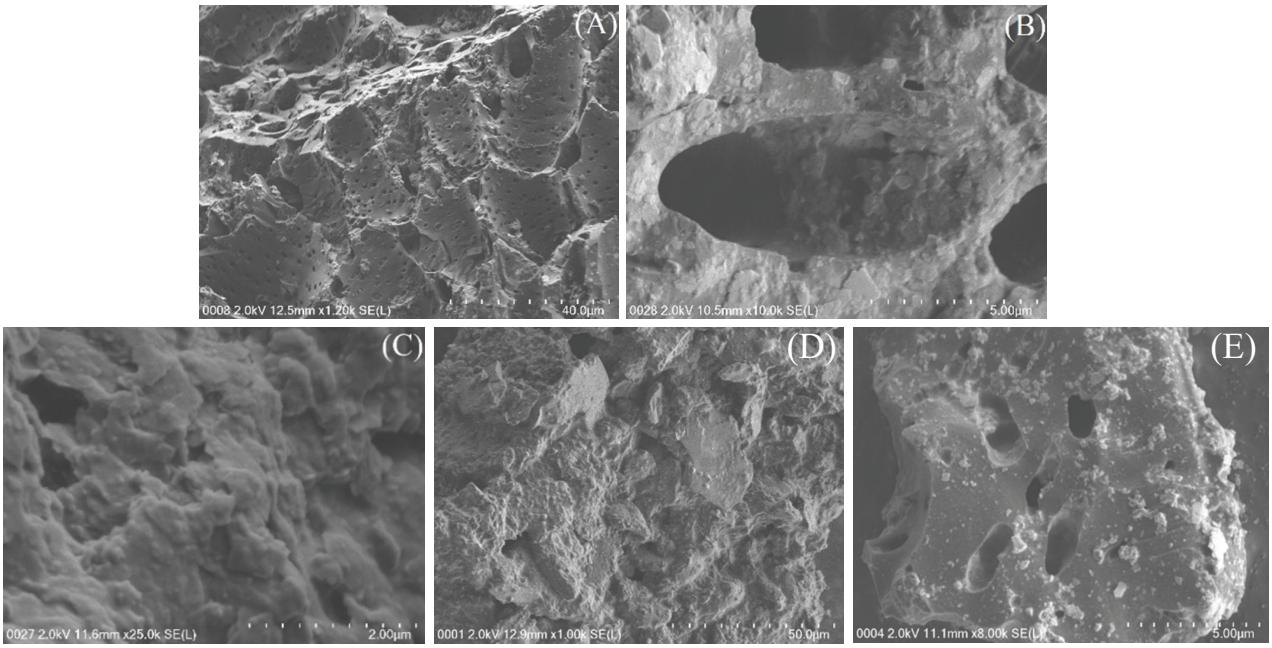

Figure 5 FESEM images of; (A) structure of the MZCS before and (B) after being applied in the smoke muffler for 30 min, (C) smoke particle clumps on the MZCS surfaces after 60 min of combustion time, (D) pure smoke sediment, and (E) MZPKS surfaces, which demonstrated poor smoke particle adsorption

Production cost estimations

The production cost estimation performed in this study was based on a similar investigation by Liew et al. (2019). The estimated costs of producing the proposed AC are tabulated in Table 5. The total process time included carbonisation and activation periods, while feedstock loading capacity was based on the furnace and microwave employed. Table 3 is also used as the reference for product yield estimations.

Feedstock, utility, and labour costs and depreciation were calculated according to the guidelines by Liew et al. (2019). Based on a lab-scale production cost approximation, this study reduced the production costs by 47%. The decrement was primarily due to the lower chemical requirement and high feedstock loading capacity. Only one low-cost chemical ($ZnCl_2$) was required for activation.

The prospective commercial implications revolved around the potential utilisation of the AC synthesised in this study to capture smoke emitted by agricultural waste combustions. The effects are more significant in situations without alternative natural waste management methods. Furthermore, future research might focus on reducing smoke emissions from municipal waste combustion processes.

CONCLUSION

The present study successfully synthesised AC suitable for smoke filter application. The AC could function as an adsorbent, filtering soot particles from the smoke produced during paddy straw combustion. The potentials of AC for smoke particle adsorption were evidenced by the FESEM images obtained in the present study. Furthermore, instantaneous adsorption led to physisorption interactions of soot with

Table 5 Cost estimations comparison with study by Liew et al. 2019

Production	Current study	Study from Liew et al. (2019)
Operating hour	8 h/day	8 h/day
Total process time	2.5 h/batch	1 h/batch
Feedstock loading capacity	5 kg	1 kg
Product yield	25 wt.% = 1.25 kg/batch	25 wt.% = 2.5 kg/batch
Daily product output	2.5 kg	2 kg
Annual product output (Five working days/week × 52 weeks/year = 260 working days yearly)	650 kg	520 kg
Operating cost		
Feedstock	USD0.05 /kg USD0.05 × 2600 kg/year = USD130 /year	USD0.05 /kg USD0.05 × 2080 kg/year = USD104 /year
Chemical	USD0.04 /kg** (USD0.04 × 2.5 kg char to produce 2.5 kg product) × 650 kg/year = USD65 /year	USD0.40 /kg (USD0.4 × 4 kg feedstock to produce 1 kg product) × 520 kg/year = USD832 /year
Utilities	USD0.03 /year 0.03 × 8 h/day × 260 days/year = USD62.4	USD0.03 /year 0.03 × 8 h/day × 260 days/year = USD62.4
Labour	USD3000/year	3000 USD/year
Depreciation	USD1283	USD1283
Annual operating cost	USD4540.4	USD5281.4
Annual operating cost/Annual output (kg/year) = Production cost	USD4.78	USD10.2

** = Estimated price on 28 January 2023 according to prices obtained from https://www.alibaba.com/product-detail/Zinc-Chloride-Chloride-Zinc-Chloride-7646_60438518441.html?spm=a2700.galleryofferlist.normal_offer.d_title.340d4558lMn5E6&s=pp

the surfaces of the AC. The production cost was reduced by approximately 47% compared to a previous study.

The CS and PKS-based AC manufactured in this study were activated with three chemical activators and microwave radiation. The ideal activator, which produced AC specimens with the highest BET values, was $ZnCl_2$. Among the AC samples acquired, the MZCS sample demonstrated superior potential as a smoke adsorbent due to its pore size and BET value. A remarkable physical adsorption level was also observed on the MZCS. Nevertheless, numerous areas regarding novel AC applications still necessitate exploration, including kinetics, isotherm and hysteresis loop types, and reusability and applications for other combustion sources. Future studies could also focus on the adsorption of smoke emitted by designated sources, such as food waste.

ACKNOWLEDGEMENT

This study was financially supported by the University of Malaya Impact-Oriented Interdisciplinary Research Grant Programme (IIRG) No. IIRG002A-19SAH.

REFERENCES

Ahmed MJ & Hameed BH. 2020. Insight into the co-pyrolysis of different blended feedstocks to biochar for the adsorption of organic and inorganic pollutants: A review. *Journal of Cleaner Production* 265: 121762. DOI: https://doi.org/10.1016/j.jclepro.2020.121762

Akbari MZ, Thepnuan D, Wiriya W et al. 2021. Emission factors of metals bound with PM2.5 and ashes from biomass burning simulated in an open-system combustion chamber for estimation of open burning emissions. *Atmosospheric Pollution Research* 12: 13–24. DOI: https://doi.org/10.1016/j.apr.2021.01.012

Atinkut HB, Yan T, Arega Y & Raza MH. 2020. Farmers' willingness-to-pay for eco-friendly agricultural waste management in Ethiopia: A contingent valuation. *Journal of Cleaner Production* 261. DOI: https://doi.org/10.1016/j.jclepro.2020.121211

Basu P. 2018. Biomass Characteristics. In Biomass Gasification, Pyrolysis and Torrefaction. Elsevier, Amsterdam.

Dhyani V & Bhaskar T. 2018. A comprehensive review on the pyrolysis of lignocellulosic biomass. *Renewable Energy* 129: 695–716. DOI: https://doi.org/10.1016/j.renene.2017.04.035

Ello AS, De Souza LKC, Trokourey A & Jaroniec M. 2013. Coconut shell-based microporous carbons for CO_2 capture. *Microporous and Mesoporous Materials* 180: 280–283. DOI: https://doi.org/10.1016/j.micromeso.2013.07.008

Enders A, Hanley K, Whitman T, Joseph S & Lehmann J. 2012. Characterization of biochars to evaluate recalcitrance and agronomic performance. *Bioresource Technology* 114: 644–653. DOI: https://doi.org/10.1016/J.BIORTECH.2012.03.022

Foo KY & Hameed BH. 2012. Textural porosity, surface chemistry and adsorptive properties of durian shell derived activated carbon prepared by microwave assisted NaOH activation. *Chemical Engineering Journal* 187: 53–62. DOI: https://doi.org/10.1016/j.cej.2012.01.079

Ghazali Z, Othaman R & Abdullah MP. 2012. Preparation Of Activated Carbon From Coconut Shell To Remove Aluminum And Manganese In Drinking Water. *Advances in Natural and Applied Sciences* 6: 1307–1312.

Hidayu AR & Muda N. 2016. Preparation and Characterization of Impregnated Activated Carbon from Palm Kernel Shell and Coconut Shell for CO_2 Capture. *Procedia Engineering* 148: 106–113. DOI: https://doi.org/10.1016/j.proeng.2016.06.463

Ilomuanya M, Nashiru B, Ifudu N & Igwilo C. 2016. Effect of pore size and morphology of activated charcoal prepared from midribs of *Elaeis guineensis* on adsorption of poisons using metronidazole and Escherichia coli O157:H7 as a case study. *Journal of Microscopy and Ultrastructure* 5: 32. DOI: https://doi.org/10.1016/j.jmau.2016.05.001

Jadhav A & Mohanraj G. 2016. Synthesis Of Activated Carbon From *Cocos Nucifera* of *Cocos nucifera* Leaves. *Chemistry and Chemical Technology* 10: 201–208.

Kumar NS, Grekovd Pré P & Alappat BJ. 2020. Microwave mode of heating in the preparation of porous carbon materials for adsorption and energy storage applications – An overview. *Renewable and Sustainable Energy Reviews* 124 (December 2019). DOI: https://doi.org/10.1016/j.rser.2020.109743

Li S, Xu S, Liu S, Yang C & Lu Q. 2004. Fast pyrolysis of biomass in free-fall reactor for hydrogen-rich gas. *Fuel Process Technology* 85: 1201–1211. DOI: https://doi.org/10.1016/j.fuproc.2003.11.043

Liew RK, Chai C, Yek PNY et al. 2019. Innovative production of highly porous carbon for industrial effluent remediation via microwave vacuum pyrolysis plus sodium-potassium hydroxide mixture activation. *Journal of Cleaner Production* 208: 1436–1445. DOI: https://doi.org/10.1016/j.jclepro.2018.10.214

Ma Y. 2017. Comparison of activated carbons prepared from wheat straw via $ZnCl_2$ and KOH activation. *Waste and Biomass Valorisation* 8: 549–559. DOI: https://doi.org/10.1007/s12649-016-9640-z

Mohd Iqbaldin MN, Khudzir I, Mohd Azlan MI, Zaidi AG, Surani B & Zubri Z. 2013. Properties of coconut shell activated carbon. *Journal of Tropical Forest Science:* 25(4): 497–503

Nasri NS, Sidik HU, Zaini MAA et al. 2019. Kinetic equilibrium and isotherm modeling adsorbed methane assessment on synthesized peek-porous sorbent carbon of sustainable coconut shell kernel. *Chemical Engineering Transactions* 72(July 2018): 247–252. DOI: https://doi.org/10.3303/CET1972042

Phairuang W, Suwattiga P, Chetiyanukornkul T et al. 2019.

The influence of the open burning of agricultural biomass and forest fires in Thailand on the carbonaceous components in size-fractionated particles. *Environmental Pollution* 247: 238–247. DOI: https://doi.org/10.1016/j.envpol.2019.01.001

Pisupati SV & Krishnamoorthy V. 2017. Utilization of coal in IGCC systems. Pp 83–120 in Wang T & Stiegel G (eds) *Integrated Gasification Combined Cycle (IGCC) Technologies*. Woodhead Publishing, Sawston.

Pósfai M, Simonics R, Li J, Hobbs PV & Buseck PR. 2003. Individual aerosol particles from biomass burning in southern Africa: 1. Compositions and size distributions of carbonaceous particles. *Journal of Geophysical Research: Atmospheres* 108: 1–13. DOI: https://doi.org/10.1029/2002jd002291

Prauchner MJ, Sapag K. & Rodríguez-Reinoso F. 2016. Tailoring biomass-based activated carbon for CH_4 storage by combining chemical activation with H_3PO_4 or $ZnCl_2$ and physical activation with CO_2. *Carbon* 110: 138–147. DOI: https://doi.org/10.1016/j.carbon.2016.08.092

Rugayah AF, Astimar AA. & Norzita N. 2014. Preparation and Characterization of Activated Carbon from Palm Kernal Shell by Physical Activation with Steam. *Journal of Oil Palm Research*. 26: 251–264.

Saka C. 2012. BET, Tg-Dtg, Ft-Ir, SEM, iodine number analysis and preparation of activated carbon from acorn shell by chemical activation with $ZnCl_2$. *Journal of Analytical and Applied Pyrolysis* 95: 21–24. DOI: https://doi.org/10.1016/j.jaap.2011.12.020

Sanchez-Silva L, López-González D, Villaseñor J, Sánchez P & Valverde JL. 2012. Thermogravimetric-mass spectrometric analysis of lignocellulosic and marine biomass pyrolysis. *Bioresource Technolology* 109: 163–172. DOI: https://doi.org/10.1016/j.biortech.2012.01.001

Sanni ES, Emetere ME, Odigure JO, Efeovbokhan VE, Agboola O & Sadiku ER. 2017. Determination of optimum conditions for the production of activated carbon derived from separate varieties of coconut shells. *International Journal of Chemical Engineering* DOI: https://doi.org/10.1155/2017/2801359

Sarkar DL. 2015. *Thermal Power Plant*. Elsevier, Amsterdam.

Shukla SK, Al Mushaiqri NRS, Al Subhi HM, Yoo K & Al Sadeq H. 2020. Low-cost activated carbon production from organic waste and its utilization for wastewater treatment. *Applied Water Science* 10: 1–9. DOI: https://doi.org/10.1007/s13201-020-1145-z

Soh M, Chew JJ, Liu S & Sunarso J. 2019. Comprehensive Kinetic Study on the Pyrolysis and Combustion Behaviours of Five Oil Palm Biomass by Thermogravimetric-Mass Spectrometry (TG-MS) Analyses. *Bioenergy Research* 12: 370–387. DOI: https://doi.org/10.1007/s12155-019-09974-9

Stampfer O, Austin E, Ganuelas T, Fiander T, Seto E. & Karr CJ. 2020. Use of low-cost PM monitors and a multi-wavelength aethalometer to characterize PM2.5 in the Yakama Nation reservation. *Atmospheric Environment* 224 (December 2019) 117292. DOI: https://doi.org/10.1016/j.atmosenv.2020.117292

Tipayarom A & Kim Oanh NT. 2020. Influence of rice straw open burning on levels and profiles of semi-volatile organic compounds in ambient air. *Chemosphere* 243, 125379. DOI: //doi.org/10.1016/j.chemosphere.2019.125379

Tounsadi H, Khalidi A, Machrouhi A et al. 2016. Highly efficient activated carbon from *Glebionis coronaria* L. biomass: Optimization of preparation conditions and heavy metals removal using experimental design approach. *Journal of Environmental Chemical Engineering* 4: 4549–4564. DOI: https://doi.org/10.1016/j.jece.2016.10.020

Wang X, Qiaoqiao C, Xuejiao L & Yin W. 2019. Influence of pyrolysis temperature on characteristics and environmental risk of heavy metals in pyrolyzed biochar made from hydrothermally treated sewage sludge. *Chemosphere* 216: 698–706. DOI: https://doi.org/10.1016/J.CHEMOSPHERE.2018.10.189

Yaacoubi H. & Songlin Z. 2019. Effect of ammonia modification on activated carbons for the removal of acidic anthraquinone dyes. *International Journal of Chemical Reactor Engineering* 17. DOI: https://doi.org/10.1515/ijcre-2018-0216

Yang K, Peng J, Xia H, Zhang L, Srinivasakannan C. & Guo S. 2010. Textural characteristics of activated carbon by single step CO_2 activation from coconut shells. *Journal of the Taiwan Institute of Chemical Engineers* 41: 367–372. DOI: https://doi.org/10.1016/j.jtice.2009.09.004

Zailani R, Ghafar H & So'aib MS. 2013. The influence of oxygen in the carbonization of oil palm shell on bio-char yield and properties. *Applied Mechanics and Materials* 393: 499–504. DOI: https://doi.org/10.4028/www.scientific.net/amm.393.499